IOP Publishing Journal of Geophysics and Engineering
J. Geophys. Eng. **13** (2016) S74–S87 doi:10.1088/1742-2132/13/2/S74

Phase-detection measurements in free-surface turbulent shear flows

Hubert Chanson

The University of Queensland, School Civil Engineering, Brisbane QLD 4072, Australia

E-mail: h.chanson@uq.edu.au and www.uq.edu.au/~e2hchans/

Received 23 December 2014, revised 26 May 2015
Accepted for publication 8 June 2015
Published 30 March 2016

Abstract

High-velocity self-aerated flows are described as 'white waters' because of the entrained air bubbles. The air entrainment induces a drastic change in the multiphase flow structure of the water column and this leads to significant bubble-turbulence interactions, turbulence modulation and associated mixing processes impacting on the bulk flow properties. In these high-velocity free-surface turbulent flows, the phase-detection needle probe is a most reliable instrumentation. The signal processing of a phase-detection probe is re-visited herein. It is shown that the processing may be performed on the raw probe signal as well as the thresholded data. The latter yields the time-averaged void fraction, the bubble count rate, the particle chord time distributions and the particle clustering properties within the particulate flow regions. The raw probe signal analysis gives further the auto-correlation time scale and the power spectrum density function. Finally dimensional considerations are developed with a focus on the physical modelling of free-surface flows in hydraulic structures. It is argued that the notion of scale effects must be defined in terms of some specific set of air–water flow properties within well-defined testing conditions, while a number of free-surface flow characteristics are more prone to scale effects than others, even in large-size physical facilities.

Keywords: high-velocity free-surface turbulent flows, phase-detection probes, signal processing, data analysis, air bubble entrainment, dimensional analysis, scale effects

(Some figures may appear in colour only in the online journal)

Introduction

In hydraulic engineering, high-velocity self-aerated flows are often described as 'white waters' because of the entrained air (figure 1) (Rao and Kobus 1971, Wood 1991, Chanson 1997). The air entrainment is caused by turbulence acting next to the air–water free-surface. Through the interface, air is continuously being trapped and released, and the air–water mixture may extend to the entire (air-) water column. Air bubble entrainment requires the turbulent shear stress to be large enough to overcome both surface tension and buoyancy effects (Ervine and Falvey 1987, Chanson 2013a). Experimental evidences showed that the free-surface of turbulent flows exhibits some surface 'waves' with fine-grained turbulent structures and larger underlying vortices, and air entrainment may result from the action of high intensity turbulent shear close to the free-surface (Brocchini and Peregrine 2001, Chanson 2009). The air entrainment induces a drastic change in the (gas–liquid) flow structure and its distribution within the water column that have direct implications in terms of turbulence modulation, bubble-turbulence interactions and associated turbulent mixing processes (Bombardelli 2012, Chanson 2013b). The interest for air–water flow measurements in high-velocity self-aerated flows is evidenced by the number of peer-reviewed articles papers published in the Journal of Hydraulic Engineering (ASCE), Journal of Hydraulic Research (Taylor & Francis), International Journal of Multiphase Flow (Elsevier), and Environmental Fluid Mechanics (Springer). For example, during the period January 2001 to November 2014, these four international scientific journals published 369 papers on air–water flows, including 114 articles on air–water flow measurements (table 1). This interest is associated to frequent citations of very early contributions. For example, the

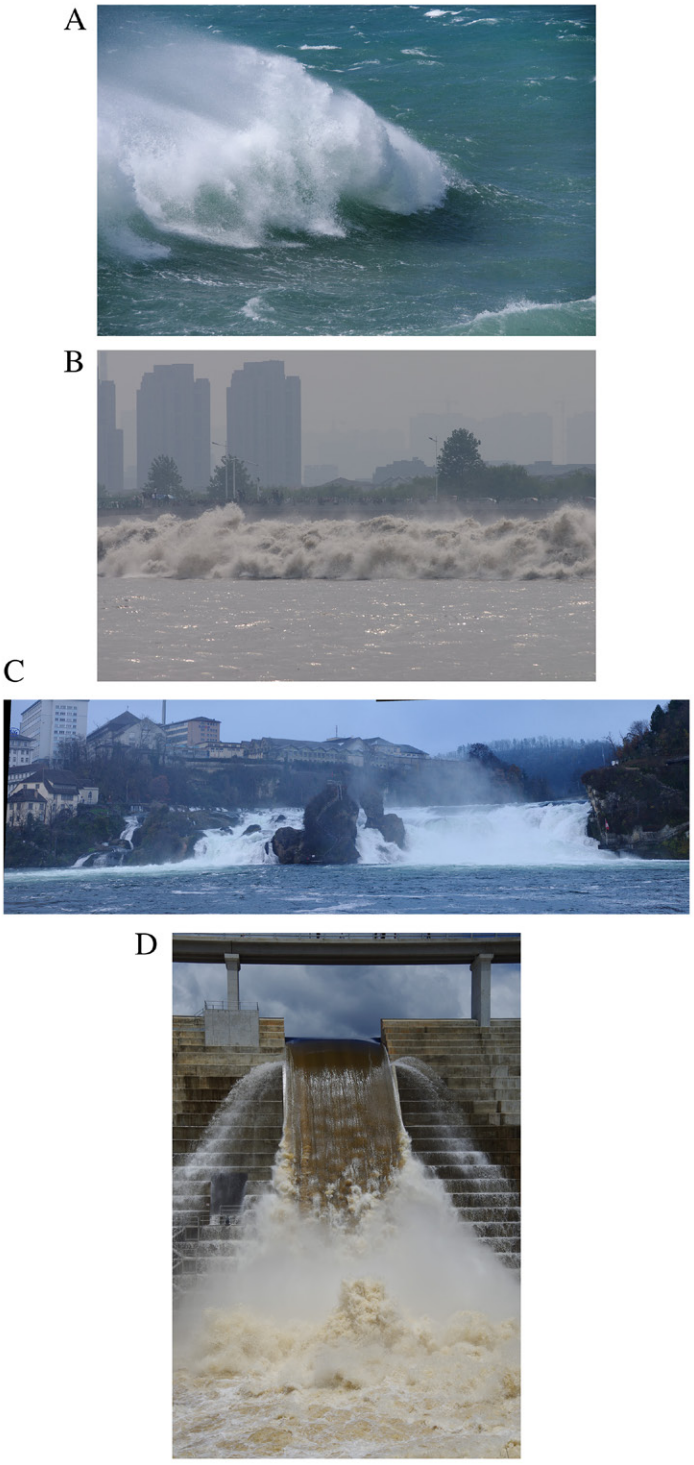

Figure 1. High-velocity air–water flows in engineering and environmental applications. (A) Breaking wave in Penghu Bay, Makong City, Makong Island, Penghu (Taiwan) on 15 January 2014 (shutter speed: 1/8000 s). (B) Qiantang River bore reflection at Laoyanchang, Hangzhou (China) on 11 October 2014 (shutter speed: 1/2000 s). (C) Rhine River waterfall ('Rheinfall') at Schaffhausen (Switzerland) on 30 November 2013. (D) Hinze dam stepped spillway operation on 29 January 2013, Nerang (Australia) (shutter speed: 1/2000 s)—flow conditions: $\theta = 51.3°$, $h = 1.2$ m, $q = 16.6\,m^2\,s^{-1}$, $d_c/h = 2.53$, Re = 1.7×10^7.

experimental study of Straub and Anderson (1958) was cited 22 times between 2001 and 2014; its re-analysis by Wood (1983) was cited 11 times over the same period (source: Web of Science™).

Despite some recent studies (Chanson 2002, Chanson and Carosi 2007, Felder and Chanson 2015), the interpretation of air–water flow data in high-velocity self-aerated flows remains poorly understood. In this contribution, the basic data processing methods are reviewed and discussed to show readily accessible information on air–water flow properties. The performances of a number of signal processing techniques applied to phase-detection conductivity probe signals

Table 1. Number of peer-reviewed research publications on air–water flows and measurements in four leading scientific journals (since 1 January 2001).

	Number of articles in			
Topic	Journal of hydraulic engineering	Journal of hydraulic research	International journal of multiphase flow	Environmental fluid mechanics
ISSN	0733-9429	0022-1686	0301-9322	1567-7419
Journal impact factor[a]:	1.258	1.347	1.943	1.164
Air water flow	65	65	216	23
Air water flow measurement	13	20	70	11

[a] 2013 Impact Factor in Web of Science.
Note: Number of articles listed in Web of Science (accessed on 16 Nov. 2014).

are compared. It is the purpose of this contribution to show the large amount of available information using electrical needle probes.

Instrumentation and measurement processing

Presentation

Most high-velocity air–water flows are characterised by large amounts of entrained air (figures 1 and 2). Figure 1 shows some prototype applications and figure 2 presents some laboratory experiments under controlled flow conditions. In these flows, the void fractions range from a few percents to nearly 100% in the upper spray region, and the ratios of flow velocity to bubble rise velocity are commonly greater than 10–20. Classical measurement techniques are adversely affected by the presence of air bubbles and air–water interfaces, and they can produce highly inaccurate readings: e.g. pointer gauge, Pitot tube, acoustic Doppler velocimeter (ADV), laser Doppler anemometer (LDA), particle image velocimetry (PIV) (Jones and Delhaye 1976, Chanson 2013b). When the void fraction C, or liquid fraction $(1 - C)$, exceeds about 1–3%, the most reliable metrology is the intrusive phase detection needle probes, notably the optical fibre probe and conductivity/resistivity probe (Cartellier and Achard 1991, Bachalo 1994, Chanson 2002), although new flow visualization techniques may allow qualitative and quantitative observations (Mossa and Tolve 1998, Leandro *et al* 2012). Intrusive probes are designed to pierce bubbles and droplets and their design is typically based upon the needle probe design developed by Neal and Bankoff (1963, 1965). Such probes have been used for over 50 years, including some milestone prototype measurements on the Aviemore Dam spillway in New Zealand (Cain and Wood 1981a, 1981b).

The principle behind the optical fibre probe is a change in optical index between the two phases (Cartellier 1992, Cartellier and Barrau 1998). The conductivity/electrical probe works based upon the difference in electrical resistivity between air and water (Herringe 1973, Serizawa *et al* 1975). There are a number of needle probe designs: single tip, dual-tip, three-tip and four-tip probes. Herein the focus is on the response of both single sensor and dual-tip probe operation.

Signal processing

In a bubbly flow, the basic two-phase flow characteristics are the void fraction and bubble density. The void fraction is defined as the volume of air per unit volume of air and water. The bubble density is the number of bubbles per unit volume. Some volume-averaged measurements are feasible with Gamma-ray and tomography, although these equipments are cumbersome and expensive.

In contrast, a needle probe is a phase-detection system which provides a point measurement of the time-variation of air or water presence (figure 3). Figure 3(A) shows a typical probe output. Each vertical signal drop corresponds to a water-to-air interface being pierced by the probe tip. Although the probe signal should be theoretically rectangular, the probe response is not exactly square because of the finite size of the tip, the wetting/drying time of the interface covering the tip and the response time of the probe and electronics.

With a needle probe, the sensor size must be small compared to the typical air/water chords, to detect the successive passage of air–water interfaces. When the slip velocity is small compared to the convection velocity, as in high-velocity self-aerated steady flows, the cumulative air chord time per unit time equals the time-averaged void fraction C and the air–water phase detection equals the instantaneous void fraction c:

$$C = \frac{1}{N} \sum_{1}^{N} c \tag{1}$$

where N is the number of samples and c is the instantaneous void fraction: $c = 0$ (water) or 1 (air).

Dual-tip probe and signal analysis

With a dual-tip phase-detection probe, also called double-tip probe (figure 4), the interfacial velocity may be analysed from the successive detection of the same interfaces by the probe sensors. In very-low void and liquid fractions, some signal pattern recognition may be used to record the spatially-averaged travel time of each interface between the sensors, albeit based upon some assumptions (Liu and Bankoff 1993). A more appropriate technique in free-surface turbulent flows is based upon a cross-correlation technique (Cain and Wood 1981a, Crowe *et al* 1998). The time-averaged interfacial velocity V is calculated from the cross-correlation function between the probe signals.

$$V = \frac{\Delta x}{T} \tag{2}$$

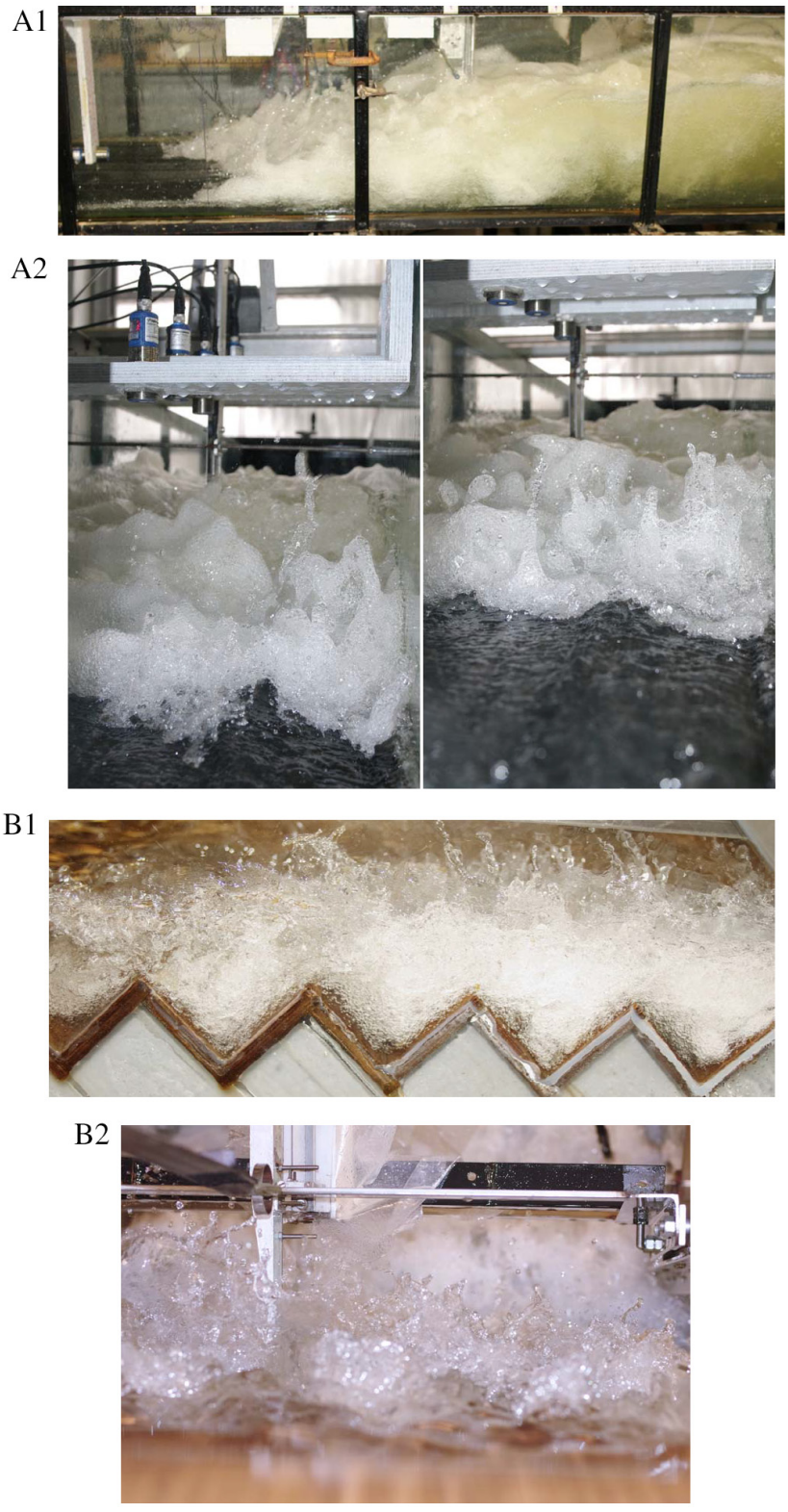

Figure 2. Laboratory investigations of air–water free-surface flows. (A) Air entrainment in hydraulic jump—flow conditions: q = 0.080 m^2 s^{-1}, d_1 = 0.020 m, x_1 = 0.83 m, Fr_1 = 8.5, Re = 7.9 × 10^4. (A1) Side view with flow direction from left to right. (A2) Looking downstream at the impingement point, roller and spray region—flow direction from foreground to background. (B) Skimming on a stepped spillway—flow conditions: θ = 45°, h = 0.1 m, q = 0.116 m^2 s^{-1}, d_c/h = 1.1, Re = 1.2 × 10^5. (B1) Side view with flow direction from left to right (shutter speed: 1/125 s). (B2) Looking downstream at the upper spray region, splashes and droplets—note the needle probe support on the left, in the background.

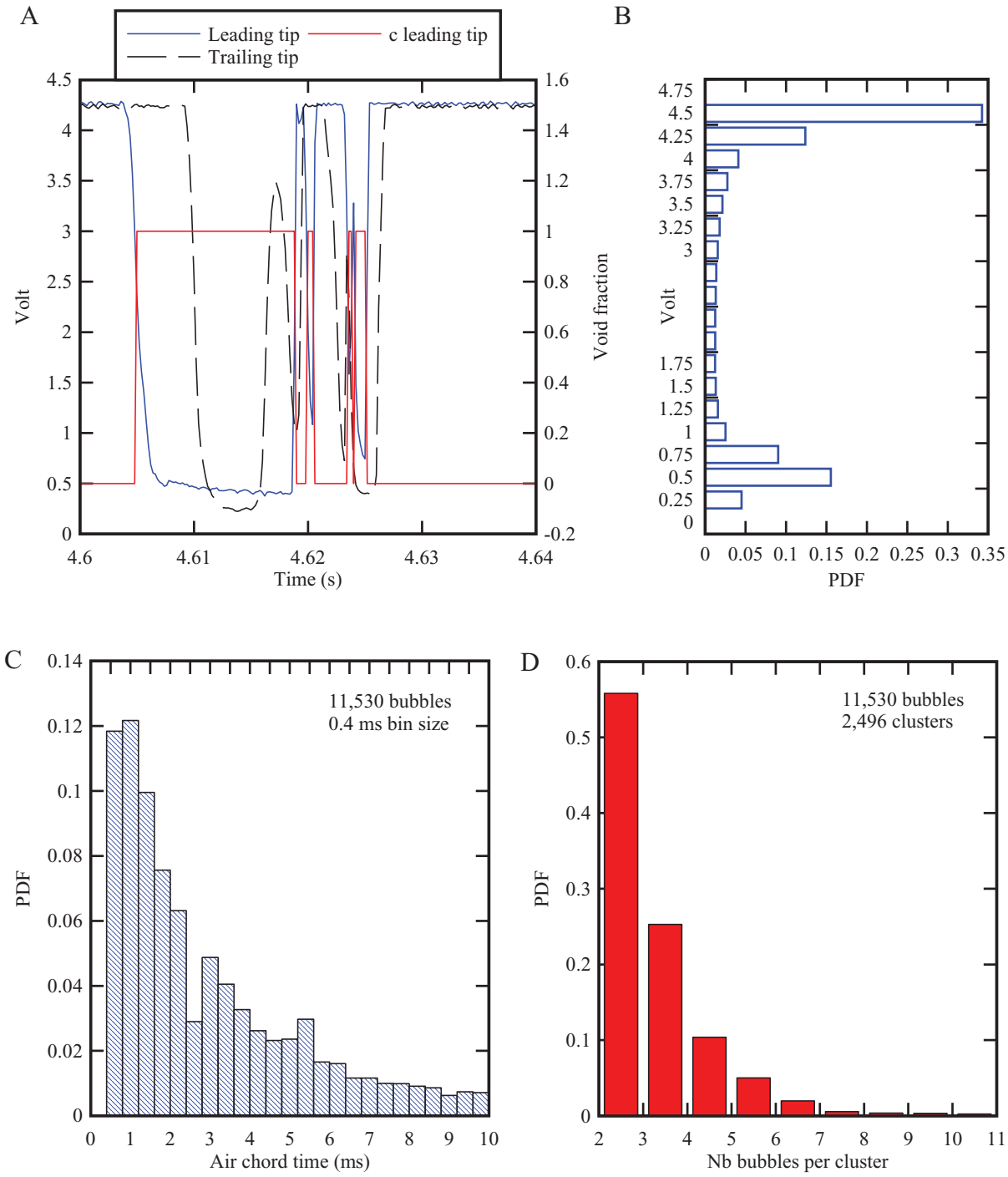

Figure 3. Single threshold analysis of conductivity probe signal output in a hydraulic jump—flow conditions: $q = 0.109\,m^2\,s^{-1}$, $d_1 = 0.0393$, $Fr_1 = 4.4$, $Re = 1.1 \times 10^5$, $x - x_1 = 0.150\,m$, $y = 0.059\,m$, 181.52 s record, sampling rate: 5 kHz, leading tip signal analysis: $C = 0.389$, $F = 63.5\,Hz$, 11 530 bubbles. (A) Raw signal and 50% thresholded signal. (B) Histogram of signal voltage (whole record). (C) PDF of bubble chord times (whole record). (D) PDF of bubble numbers per cluster (whole record).

where T is the average interfacial travel time between the sensors corresponding to the time lag of the maximum cross-correlation function $(R_{xy})_{max}$ and Δx is the distance between probe sensors (figure 4).

The shape of the auto- and cross-correlation functions may provide further characteristics, including the cross-correlation time scales (figure 4(B)) and the turbulence intensity (Chanson and Toombes 2002a, Chanson and Carosi 2007, Felder and Chanson 2014).

Effects of sampling rate and duration

The effects of sampling frequency and duration were tested in a number of studies using the single-threshold technique.

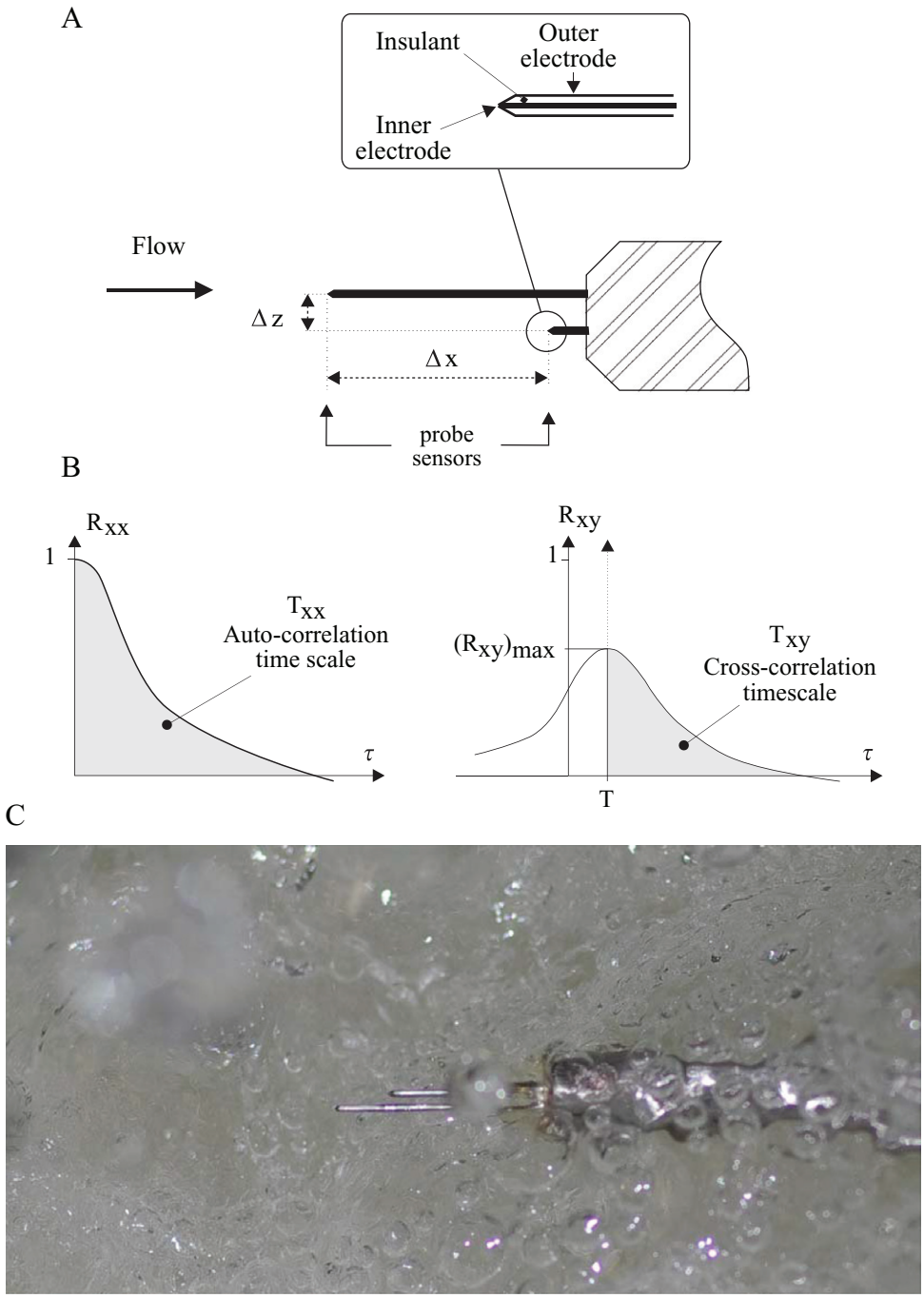

Figure 4. Dual-tip phase-detection probes and cross-correlation function between probe tip signals: definition sketches and photograph. (A) Probe design, viewed in elevation. (B) Normalised auto- and cross-correlation functions. (C) Dual-tip phase-detection probe in operating in the upper spray region of a hydraulic jump with $Fr_1 = 7.5$ (inner electrode ∅: 0.25 mm, $\Delta x \sim 7$ mm)—view in elevation, mean flow direction from left to right.

Table 2 regroups the main characteristics of studies conducted in high-velocity self-aerated flows, including the instrumentation and flow conditions. It summarises the key findings in table 2 (Last column).

A key outcome is that the effects of sampling rate and duration differ significantly depending upon the type of two-phase flow parameter. Generally the void fraction is a robust parameter, least affected by the sampling conditions. On the other hand, the bubble count rate, turbulence intensity, correlation time scales and clustering properties are more sensitive to the sampling parameters.

Basic signal analyses

Presentation

A number of phase discrimination techniques were developed, including single-threshold, double-threshold, signal slopes

Table 2. Summary of systematic sensitivity analyses conducted with phase-detection probes in high-velocity self-aerated flows.

Reference	Instrumentation	Flow conditions	Air–water property	Outcome
Cummings (1996)	Dual tip conductivity probe (Ø = 0.025 mm) T_{scan} = 2 s F_{scan} = 40 kHz	2D supported plunging jet (d_1 = 12 mm) 0.3 < V_1 < 9 m s^{-1}	Void fraction	Threshold level: 20%–70% of air–water range
Toombes (2002)	Single tip conductivity probe (Ø = 0.35 mm) 3 < T_{scan} < 180 s Dual tip conductivity probe (Ø = 0.025 mm) 3 < T_{scan} < 100 s 6 < F_{scan} < 80 kHz	Supercritical flow past an abrupt drop (h = 0.143 m) 2 < Fr_1 < 10 2.6 × 10^5 < Re < 5.6 × 10^5	Void fraction	Threshold level: 40%–60% of air–water range F_{scan} > 6 kHz T_{scan} > 10 s
		Supercritical flow past an abrupt drop (h = 0.143 m) 2 < Fr_1 < 10 2.6 × 10^5 < Re < 5.6 × 10^5	Bubble chord size	F_{scan} > 5–40 kHz T_{scan} > 10 s
Chanson (2007)	Single tip conductivity probe (Ø = 0.35 mm) 0.7 < T_{scan} < 300 s 0.6 < F_{scan} < 80 kHz	Hydraulic jumps 5.1 < Fr_1 < 8.5 1 × 10^5 < Re < 4 × 10^5	Void fraction	F_{scan} > 600 Hz T_{scan} > 30–40 s
			Bubble count rate	F_{scan} > 6–8 kHz T_{scan} > 30–40 s
Chanson and Felder (2010)	Single tip conductivity probe (Ø = 0.35 mm) & dual-tip conductivity probe (Ø = 0.25 mm) T_{scan} = 45 s F_{scan} = 20 kHz	Skimming flow on stepped spillway θ = 26.6°, h = 0.10 m 0.7 < d_c/h < 1.45 2.3 × 10^5 < Re < 6.9 × 10^5	Void fraction	Threshold level: 25%–85% of air–water range
			Bubble count rate	Threshold level: 40%–60% of air–water range
Felder (2013) (also Felder and Chanson 2015)	Dual-tip conductivity probe (Ø = 0.25 mm) 1 < T_{scan} < 180 s 1 < F_{scan} < 40 kHz	Skimming flow on stepped spillway θ = 26.6°, h = 0.10 m 0.7 < d_c/h < 1.45 2.3 × 10^5 < Re < 6.9 × 10^5	Void fraction	T_{scan} > 20 s F_{scan} > 1 kHz
			Bubble count rate	T_{scan} > 20–40 s F_{scan} > 10 kHz
			Interfacial velocity	T_{scan} > 20–40 s F_{scan} > 5 kHz
			Turbulence intensity	T_{scan} > 20–40 s F_{scan} > 10 kHz
			Correlation time scales	T_{scan} > 20–40 s
Wuthrich and Chanson (2014)	Dual-tip conductivity probe (Ø = 0.25 mm) 1 < T_{scan} < 180 s 1 < F_{scan} < 100 kHz	Skimming flow on stepped spillway θ = 26.6°, h = 0.10 m, gabions d_c/h = 1.3, Re = 6 × 10^5	Void fraction	Threshold leve: 30%–80% of air–water range T_{scan} > 20 s F_{scan} > 1 kHz
			Bubble count rate	Threshold level: 40%–60% of air–water range T_{scan} > 20 s F_{scan} > 20 kHz
			Interfacial velocity	T_{scan} > 20 s
			Turbulence intensity	T_{scan} > 40 s

Note: d_1: inflow depth; d_c: critical flow depth; F_{scan}: sampling rate per sensor; h: vertical step height; Fr_1: inflow Froude number; Re: Reynolds number defined in terms of the hydraulic diameter; T_{scan}: sampling duration; V_1: inflow velocity.

and signal curvatures (Lance and Bataille 1991, Cartellier 1992, Cummings 1996). A simple signal analysis is based upon the single threshold technique and figure 3 illustrates a typical application. The probability distribution function (PDF) of the raw probe signal is bi-modal (figure 3(B)). In self-aerated free-surface flows, a very robust technique is the single-threshold technique, with a threshold set at 50% of the air–water range for all elevations (Toombes 2002, Chanson and Carosi 2007). The single threshold level is defined relative to the air–water range which is determined by the signal voltage modes. Some very early studies linked the threshold level to the local void fraction as discussed by Jones and Delhaye (1976). For example, a low threshold may be used in bubbly flows with very fine bubble sizes (Chanson *et al* 2002). The effects of threshold level on the air–water flow properties were tested (Herringe and Daves 1974, Toombes 2002, Chanson and Felder 2010, Felder 2013, Wuthrich and Chanson 2014, Felder and Chanson 2015). The results showed little effect for a threshold between 40 and 60% of the air–water range. This threshold level must be applied to all the data set. Figure 3(A) illustrates the application of the 50% threshold to a truncated signal. The thresholded signal is the instantaneous void fraction c with a square-wave shape between 0 and 1 (figure 3(A), Red). Sometimes, short events are not recorded as interfacial changes. A number of more advanced phase discrimination technique are discussed by Jones and Delhaye (1976) and Cartellier and Achard (1991) (also Chanson and Brattberg (1998), Rensen *et al* (2005) and Bung (2012)).

The thresholded signal, or time variation of instantaneous void fraction, is used to calculate the void fraction, bubble count rate, air and water chord time distributions and particle clustering properties. In a steady stationary flow, the time-averaged void fraction C is the arithmetic mean of the instantaneous void fraction (equation (1)). The bubble count rate F is the number of bubbles (i.e. water-to-air interfaces) detected by the probe sensor per second. For the entire record illustrated in figure 3, this yields $C = 0.389$ and $F = 63.5$ Hz.

When $C < 0.3$–0.4 as for the data set shown in figure 3, the air–water flow consists typically of air bubbles surrounded by a water medium. The normalised probability distribution function of bubble chord times is presented in figure 3(C), in which the histogram columns represent the probability of a bubble chord time in 0.4 ms intervals: e.g. the probability of a chord length from 0.4 to 0.8 ms is represented by the column labelled 0.4. The experimental data showed a broad range of bubble chord times. The PDF was skewed with a preponderance of small chord times compared to the mean and it exhibited a similar shape to a number of standard PDFs including the Gamma, Weibull and log-normal PDFs, as previously documented in self-aerated free-surface flows (Chanson and Toombes 2002a, Toombes and Chanson 2008).

The streamwise distribution of air and water chord times may provide some information on particle clustering. The notion of particle clustering is only meaningful in a particulate flow: that is, in the bubbly flow region ($C < 0.3$) and spray region ($C > 0.7$) of self-aerated flows, following Chanson and Toombes (2002a). A cluster of particles is defined as a group of two or more particles, with a distinct separation from other particles before and after the cluster. The study of particle clustering is relevant in industrial applications to infer whether the cluster formation frequency responds to some particular frequencies of the flow (Noymer 2000, Heinlein and Fritsching 2006, Calzavarini *et al* 2008a). The clustering index may provide a measure of the vorticity production rate and associated energy dissipation, while the level of clustering may give some indication of the magnitude of bubble-turbulence interactions and associated turbulent dissipation. Considering a group of two bubbles, the trailing particle may be in the near-wake of and affected by the lead bubble. For a bubble rising in still water, the wake length is about 0.5 to 2 times the particle size at large-particle Reynolds numbers (Clift *et al* 1978). The near wake clustering criterion is very effective because it relies on a comparison between the local characteristic flow times (Chanson 2002b, Chanson *et al* 2006, Gualtieri and Chanson 2010). Following Chanson *et al* (2006), two successive bubbles are defined as a cluster when the trailing bubble is separated from the lead bubble by a water chord time smaller than one leading bubble chord time. A typical result is presented in figure 3(D) in terms of the PDF of number of bubbles per cluster. Overall 60.4% of bubbles were in some cluster structure, with an average of 2.8 bubbles per cluster for this data set. Note that this approach is restricted to the longitudinal distribution of particles and does not take into account particles travelling side by side or a group of spatially distributed particles. A recent numerical study showed that the longitudinal signal analysis may be representative of the 3D flow (Calzavarini *et al* 2008b), while an experimental study of 2D clustering highlighted some complex interactions between entrained air and turbulent structures (Sun and Chanson 2013).

Some further signal analysis of the raw voltage may yield the auto-correlation time scale and the power spectrum density function. The autocorrelation function provides some information on the air–water flow characteristics, in the form of a measure of the air–water flow coherence and 'memory'. Its integration up to the first crossing gives a characteristic time scale of the air–water flow structures:

$$T_{xx} = \int_0^{\tau=\tau(R_{xx}=0)} R_{xx} \times \mathrm{d}\tau \tag{3}$$

where R_{xx} is the normalised auto-correlation function and τ is the time lag. Figure 5(A) presents some typical auto-correlation functions and the data analysis results are given in the figure caption.

A Fourier spectral analysis gives additional information on the frequency distribution of the signal that is related to the air + water time scale distribution. Considering the bubble striking at the probe sensor as a stochastic process, the auto power spectrum may provide some information on the stationarity and periodicity of the signal (Chanson and Gonzalez 2004, Gonzalez 2005). Figure 5(B) illustrates some typical results.

The above analyses of phase-detection probe signal do not assume any particular gas–liquid structures and may be applied across the entire water column independently of the

Y (m)	C	F Hz	T_{xx} (ms)	s_1	f_c Hz	s_2
0.131	0.115	20.1	34.2	−0.66	200	−1.44
0.159	0.368	25.6	62.3	−0.75	200	−1.57

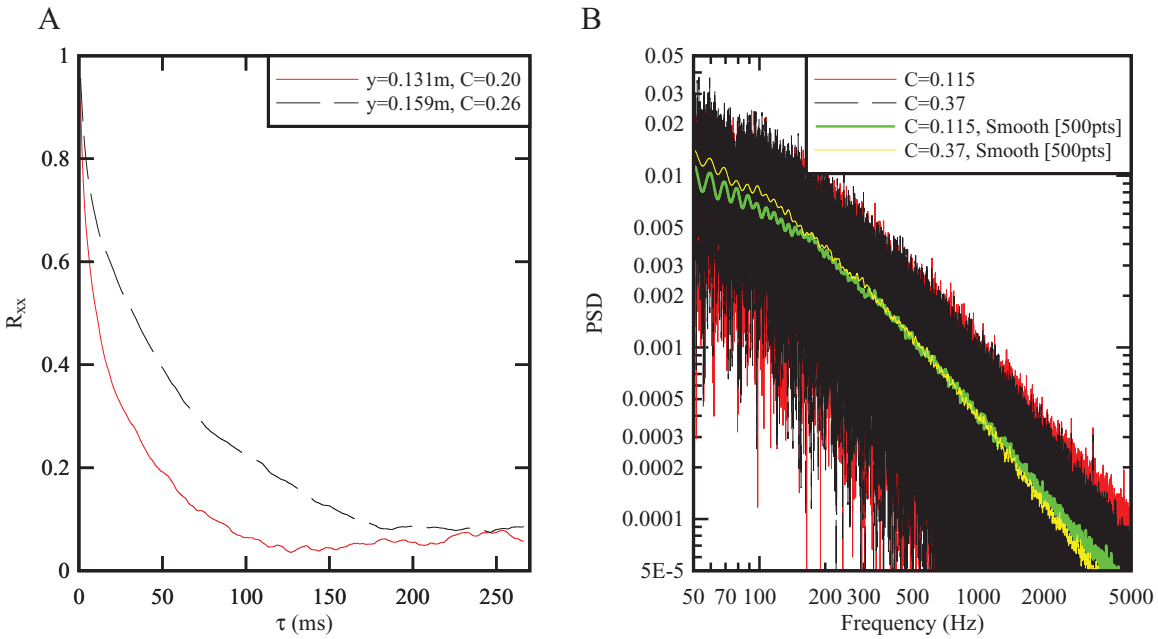

Figure 5. Auto-correlation and power spectral density (PSD) functions of raw probe signal in a hydraulic jump (leading tip signal)—flow conditions: $q = 0.1254\,m^2\,s^{-1}$, $x_1 = 1.50\,m$, $d_1 = 0.0395$, $Fr_1 = 5.1$, $Re = 1.25 \times 10^5$, $x - x_1 = 0.300\,m$, sampling rate: 20 kHz, sampling duration: 45 s. (A) Normalised auto-correlation function. (B) PSD function (up to 2 kHz).

time-averaged void fraction. An implicit assumption is the flow steadiness, although some different signal processing techniques were developed to study air entrainment in pulsating flows (Felder and Chanson 2014, Wang *et al* 2014), periodic breaking waves (Hwung *et al* 1992, Cox and Shin 2003, Hoque and Aoki 2005) and unsteady rapidly-varied flows like dam break waves (Chanson 2004, 2005) and bores (Leng and Chanson 2015).

Advanced signal analyses

The standard deviation of the instantaneous void fraction is:

$$c_{rms} = \frac{1}{N} \times \sum (c - C)^2 \quad (4)$$

The instantaneous void fraction c is either 0 or 1: namely, $c = 1$ for a proportion of time/data equals to the time-averaged void fraction C. This gives a relationship between the root mean square of the instantaneous void fraction and the time-averaged void fraction (Murai *et al* 2006):

$$c_{rms} = C \times (1 - C)^2 + (1 - C) \times C^2 = C \times (1 - C) \quad (5)$$

Equation (5) implies a parabolic relationship between time-averaged void fraction and void fraction root mean square.

In a number of free-surface aerated flows, the relationship between time-averaged void fraction and bubble count rate follows in first approximation (Chanson and Toombes 2002a, Toombes and Chanson 2008):

$$\frac{F}{F_{max}} \approx 4 \times C \times (1 - C) \quad (6)$$

where F_{max} is the maximum bubble count rate in the cross-section, typically observed for $C = 0.4$–0.5 (Toombes and Chanson 2008). Combining equations (5) and (6), it yields:

$$c_{rms} \approx \frac{1}{4} \times \frac{F}{F_{max}} \quad (7)$$

The result indicates that the void fraction root mean square is maximum for $F = F_{max}$.

A more advanced theoretical relationship between time-averaged void fraction and bubble count rate was introduced (Toombes 2002, Toombes and Chanson 2008):

$$\frac{F}{F_{max}} = \frac{1}{\alpha \times \beta} \times \frac{C \times (1 - C)}{C_{F_{max}}^2} \quad (8)$$

where α and β are two correction factors which are functions of the local void fraction and flow conditions, and C_{Fmax} is the void fraction for which $F = F_{max}$. The first correction parameter α accounts for the different average sizes of air bubble chord size λ_a and water droplet chord size λ_w:

$$\alpha = 1 + \left(\frac{\lambda_w}{\lambda_a} - 1 \right) \times C \quad (9)$$

with the ratio λ_w/λ_a assumed to be constant within a cross-section and independent of the void fraction. The second

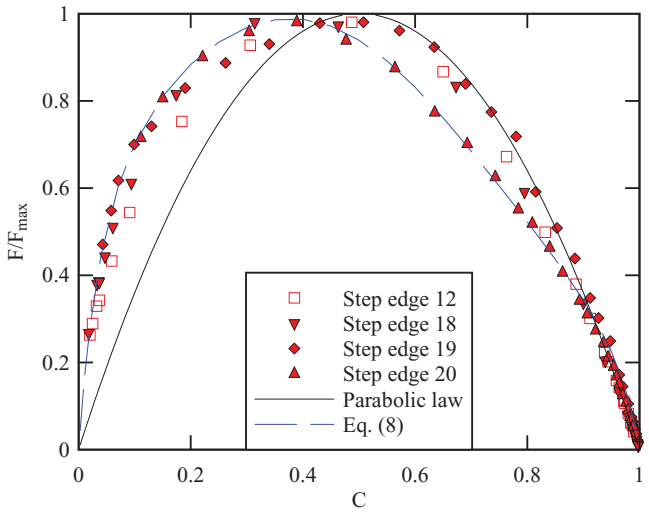

Figure 6. Relationship between bubble count rate and void fraction in high-velocity free-surface flows—flow conditions: skimming flow on smooth impervious steps, $h = 0.05$ m, $q = 0.0674\,m^2s^{-1}$, $d_c/h = 1.58$, Re = 6.7×10^4, step edges 12, 18, 19 & 20, sampling rate: 20 kHz, sampling duration: 45 s—comparison with data at step edge 20 and equations (6) and (8).

correction factor β takes into account the variation of λ_w and λ_a with the void fraction:

$$\beta = 1 - b \times (1 - 2 \times C)^4 \quad (10)$$

where b is a characteristic value of the maximum variation of β: i.e. $(1 - b) < \beta < 1$ (Toombes and Chanson 2008). Typical values of λ_w/λ_a and b were documented in self-aerated stepped chute flows (Toombes 2002, Gonzalez 2005, Toombes and Chanson 2008, Bung 2009, Felder 2013, Wuthrich and Chanson 2014) and hydraulic jumps (Wang 2014). Experimental data are presented in figure 6, in which they are compared with equations (6) and (8).

In self-aerated free-surface flows, the power spectrum distribution (PSD) of the raw probe signal may can be roughly divided in two zones, corresponding to two straight lines with different slope $s1$ and $s2$:

$$\text{PSD} \propto f^{s1} \qquad f < f_c \quad (11)$$

$$\text{PSD} \propto f^{s2} \qquad f < f_c \quad (12)$$

where f is the frequency and f_c is a characteristic frequency. Equation (11) characterises the total energy in the signal due to the largest length scales, and equation (12) describes the total energy of the signal for the smaller scales (Gonzalez 2005). Some remarkable result was obtained in skimming flows on a stepped chute (Chanson and Gonzalez 2004). Namely the exponent $s1$ showed different values at different elevations y; the finding suggested that the grouping of air + water structures with a time scale larger than $1/f_c$ varied with depth, void fraction and bubble count rate. On the other hand, the exponent $s2$ was nearly constant through all vertical profiles at all locations, suggesting that interfaces with time scales smaller than $1/f_c$ were roughly independent of, or insensitive to, the turbulent flow conditions and air–water flow properties. The characteristic frequency f_c was typically of the same order of magnitude as the bubble count rate. Some typical data are included in figure 5 for a hydraulic jump and details are provided in the figure caption.

Physical modelling, dimensional considerations and similarity

In high velocity free-surface flows, the entrainment of air bubbles may be localised at a flow discontinuity or continuous along an air–water free-surface (Kobus 1984, Wood 1991, Chanson 1997). These two dominant modes are often called singular and interfacial aeration respectively. Examples of singular aeration include the air bubble entrainment by a hydraulic jump and plunging jet (figures 1(B) and 2(A)). Interfacial aeration is defined as the air bubble entrainment process along an air–water interface, usually parallel to the flow direction (figures 1(D) and 2(B)). Any fundamental analysis of such free-surface flows is based upon a large number of relevant equations to describe the two-phase turbulent flow motion. Physical modelling may provide some information on the flow motion if a suitable dynamic similarity is selected (Novak and Cabelka 1981, Liggett 1994). The relevant dimensional parameters include the air and water physical properties and constants, the boundary conditions, the inflow and tailwater conditions, and the local two phase flow properties at a location (x, y, z) within the free-surface turbulent shear flow (Wood 1991). Note that the flow is assumed to be steady herein.

Considering the singular aeration at a hydraulic jump in a smooth horizontal rectangular channel (figure 7(A)), a simplified dimensional analysis yields:

$$C, \frac{V}{V_1}, \frac{v'}{V_1}, \frac{L_t}{d_1}, T_t \times \sqrt{\frac{g}{d_1}}, \frac{F \times d_1}{V_1}, \frac{D_{ab}}{d_1}, \frac{N_c \times d_1}{V_1}, \ldots = F_1\left(\frac{x - x_1}{d_1}, \frac{y}{d_1}, \frac{z}{d_1}, \frac{V_1}{\sqrt{g \times d_1}}, \rho \times \frac{V_1 \times d_1}{\mu}, \frac{g \times \mu^4}{\rho \times \sigma^3}, \frac{x_1}{d_1}, \frac{W}{d_1}, \frac{v_1'}{V_1}, \frac{\delta}{d_1}, \ldots\right) \quad (13)$$

where v' is a characteristic turbulent velocity, L_t an integral length scale, T_t a integral time scale, D_{ab} a characteristic bubble size, N_c the number of bubble clusters per second, d_1 the inflow depth, V_1 the inflow velocity, x the longitudinal coordinate, y the vertical elevation above the invert, z the transverse coordinate measured from the channel centreline, g the gravity constant, ρ and μ the water density and dynamic viscosity respectively, σ the surface tension between air and water, x_1 the longitudinal coordinate of the jump toe, W the channel width, v_1' a characteristic turbulent velocity at the inflow, δ the boundary layer thickness of the inflow. Equation (13) expresses the air–water flow properties at a position (x, y, z) within the jump roller as functions of the inflow properties, fluid properties and channel geometry using the upstream flow depth d_1 as the relevant length scale. In the right hand side of equation (13), the 4th, 5th and 6th terms are respectively the upstream Froude number

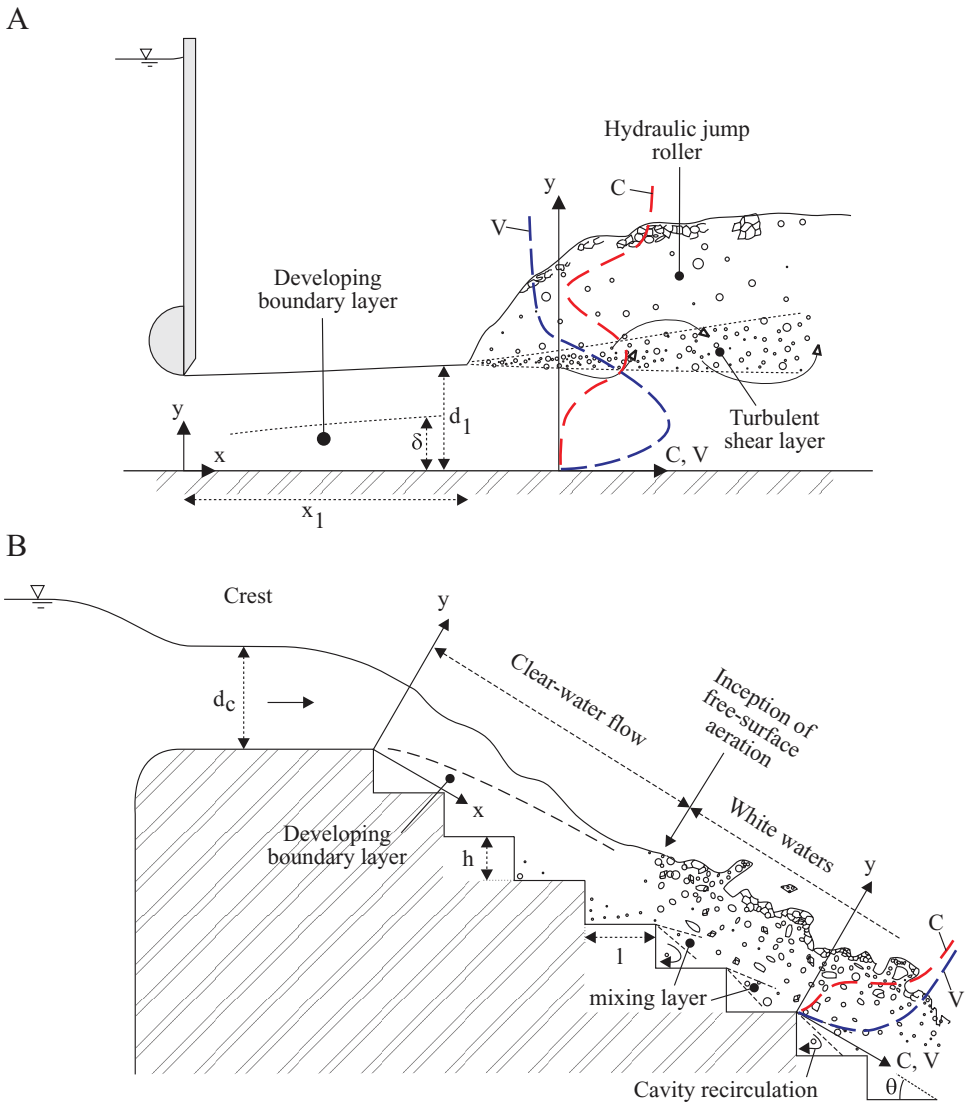

Figure 7. Free-surface turbulent shear flow: definition sketches. (A) Hydraulic jump in a rectangular channel. (B) Self-aerated skimming flow on a stepped chute.

Fr_1, the Reynolds number Re and the Morton number Mo. In a hydraulic jump, the momentum considerations demonstrate the significance of the inflow Froude number (Bélanger 1841, Lighthill 1978) and the selection of the Froude similitude derives implicitly from basic theoretical considerations (Liggett 1994, Chanson 2012). The Froude dynamic similarity is commonly applied in the hydraulic literature (Bakhmeteff and Matzke 1936, Hager 1992, Chanson and Chachereau 2013). The Reynolds number is another relevant dimensionless number because the hydraulic jump is a turbulent shear flow (Rouse *et al* 1959, Rajaratnam 1965, Hoyt and Sellin 1989). When the same fluids (air and water) are used in models and prototype as in the present study, the Morton number Mo becomes an invariant and this adds an additional constraint upon the dimensional analysis.

For the interfacial aeration of a skimming flow on a stepped spillway (figure 7(B)), basic dimensional considerations yield:

$$C, \frac{V}{V_c}, \frac{v'}{V_c}, \frac{L_t}{d_c}, T_t \times \sqrt{\frac{g}{d_c}}, \frac{F \times d_c}{V_c}, \frac{D_{ab}}{d_c}, \frac{N_c \times d_c}{V_c}, \ldots = F_2\left(\frac{x}{d_c}, \frac{y}{d_c}, \frac{z}{d_c}, \frac{d_c}{h}, \rho \times \frac{q}{\mu}, \frac{g \times \mu^4}{\rho \times \sigma^3}, \frac{W}{d_c}, \theta, \frac{k_s'}{d_c}, \ldots.\right) \quad (14)$$

where d_c is the critical flow depth is the interfacial velocity ($d_c = (q^2/g)^{1/3}$)), V_c the critical flow velocity ($V_c = (g \times d_c)^{1/2}$), q the water discharge per unit width, x, y, z are respectively the longitudinal, normal and transverse coordinates, h and l the step height and length respectively, W is the channel width, g the gravity acceleration, θ the chute slope, k_s' the equivalent sand roughness height of the step cavity boundary surface. In equation (14), the dimensionless discharge d_c/h is proportional to a Froude number defined in terms of the step height: $d_c/h = (q/(g \times h^3)^{1/2})^{2/3}$, while the 5th and 6th dimensionless terms are the Reynolds and Morton numbers respectively.

For both singular and interfacial aeration processes, it is physically impossible to fulfil simultaneously the Froude,

Reynolds and Morton similarity requirements, unless working at full scale. In practice, laboratory studies are conducted with air and water: that is, the same fluids are used in model and prototype implying a Morton similitude, while free-surface flows are studied based upon a Froude similarity (Henderson 1966, Liggett 1994). Thus the Froude and Morton dynamic similarities are simultaneously used, but the Reynolds number is underestimated in laboratory conditions. A number of studies indeed showed that the free-surface aeration is affected by adverse scale effects in small size models (Rao and Kobus 1971, Chanson 1997).

Discussion

A small number of systematic studies performed on geometrically similar models based upon the Froude and Morton similitudes showed clearly the limitations of dynamic similarity and physical modelling of free-surface turbulent shear flows (Murzyn and Chanson 2008, Felder and Chanson 2009, Pfister and Hager 2010, Chanson and Chachereau 2013). The study outcomes demonstrated that the selection of any criterion to assess scale affects is a critical issue: e.g. the distribution of void fraction, bubble count rate, turbulence intensity and many more. Any mention of scale effects must be associated with the detailed list of tested parameters and tested flow conditions (Chanson 2009, Schultz and Flack 2013). Experimental data showed that a number of properties, including bubble sizes, turbulent scales and clustering characteristics, are affected by scale effects, even in 2:1 to 3:1 scale models. No scale effect is observed at full scale only, using the same fluids in prototype and model: i.e. in prototype flow conditions.

The effects of surfactants, biochemicals and water temperature on the air entrainment process and two-phase flow properties were neglected in the above developments. Some experimental data showed some significant effect on the air–water flow properties which were implicitly ignored in the above equations (Reif 1978, Chanson *et al* 2006, Pothof *et al* 2013, Salter *et al* 2014, Callaghan *et al* 2014). The effects of intrusive probe sensors were further neglected, although findings with phase-detection needle probes suggested a non-negligible impact on the detection of small bubbles (Chanson and Toombes 2002b, Gonzalez 2005, Vejrazka *et al* 2010).

In equations (13) and (14), the Reynolds number was selected instead of the Weber number because the study focuses on the scaling of free-surface flows in prototype hydraulic structures with Reynolds numbers from 10^6 to in excess of 10^9 (figure 1). At such large Reynolds numbers, surface tension is considered of lesser significance compared to the viscous effects in free-surface turbulent shear flows (Cain and Wood 1981b, Wood 1991, Ervine 1998). Note that the Froude and Morton similarities imply: $We \propto Re^{4/3}$.

Conclusion

In high-velocity free-surface turbulent flows, the flow is most often highly aerated (figures 1 and 2) and the phase-detection needle probe is the most reliable instrument to characterise thoroughly the two-phase air–water flow properties throughout the air–water column. The signal processing of a needle probe is reviewed and it is shown that the processing may be performed on both the raw probe signal and thresholded data. The former gives further the auto-correlation time scale and the power spectrum density function. The thresholded signal analysis yields the time-averaged void fraction, the bubble count rate, the particle chord time distributions and the particle clustering characteristics within the particulate flow regions.

The results bring new details on the turbulent nature of these complex two-phase free-surface flows. Further developments are needed, including experimental, numerical and theoretical analyses. Laboratory studies under controlled conditions may deliver new information using dynamically similar models. The outcomes of recent systematic experimental studies indicated that (1) the notion of scale effects must be defined in terms of some specific set of air–water flow property(ies) within well-defined testing conditions, and (2) some free-surface flow characteristics are more prone to scale effects than others, even in large-size physical facilities. Future research must consider field measurements of high quality, because no prototype data means no definite validation of physical, numerical and theoretical models. It is believed that the bubble-turbulence interactions in free-surface flows will remain a key challenge for the 21st century.

Acknowledgments

The author thanks all his students and collaborators involved in this research topic over the last three decades. The helpful comments of the reviewers are acknowledged. The financial support through the Australian Research Council (Grant DP0878922 and DP120100481) is acknowledged.

References

Bachalo W D 1994 Experimental methods in multiphase flows *Int. J. Multiph. Flow* **20** 261–95

Bakhmeteff B A and Matzke A E 1936 The hydraulic jump in terms of dynamic similarity *Transactions* **101** 630–47

Bélanger J B 1841 Notes sur l'Hydraulique ('Notes on Hydraulic Engineering') *Ecole Royale des Ponts et Chaussées* (*Paris, France*) session 1841–2, 223 p (in French)

Bombardelli F A 2012 Computational multi-phase fluid dynamics to address flows past hydraulic structures *Proc. 4th IAHR Intl. Symp. Hydraulic structures APRH—Associação Portuguesa dos Recursos Hídricos* (*Porto, Portugal, 9–11 February*) ed J Matos *et al* 19 p (CD-ROM)

Brocchini M and Peregrine D H 2001 The dynamics of strong turbulence at free Surfaces. Part 2. Free-surface boundary conditions *J. Fluid Mech.* **449** 255–90

Bung D B 2009 Zur selbstbelüfteten Gerinneströmung auf Kaskaden mit gemäßigter Neigung *PhD Thesis* Bergische University Wuppertal, Germany, 293 p (in German)

Bung D B 2012 Sensitivity of phase detection techniques in areated chute flows to hydraulic design parameters *Proc 2nd European IAHR Congress (Munich, Germany)* 6 p (CD-ROM)

Cain P and Wood I R 1981a Instrumentation for aerated flow on spillways *J. Hydraul. Div.* **107** 1407–24

Cain P and Wood I R 1981b Measurements of self-aerated flow on a spillway *J. Hydraul. Div.* **107** 1425–44

Callaghan A H, Stokes M D and Deane G B 2014 The effect of water temperature on air entrainment, bubble plumes, and surface foam in a laboratory breaking-wave analog *J. Geophys. Res. Oceans* **119** 7463–82
Calzavarini E, Kerscher M, Lohse D and Tochi F 2008a Dimensionality and morphology of particle and bubble clusters in turbulent flow *J. Fluid Mech.* **607** 13–24
Calzavarini E, van der Berg T H, Toschi F and Lohse D 2008b Quantifying microbubble clustering in turbulent flow from single-point measurements *Phys. Fluids* **20** 040702
Cartellier A 1992 Simultaneous void fraction measurement, bubble velocity, and size estimate using a single optical probe in gas–liquid tow-phase flows *Rev. Sci. Instrum.* **63** 5442–53
Cartellier A and Achard J L 1991 Local phase detection probes in fluid/fluid two-phase flows *Rev. Sci. Instrum.* **62** 279–303
Cartellier A and Barrau E 1998 Monofiber optical probes for gas detection and gas velocity measurements: conical probes *Int. J. Multiph. Flow* **24** 1265–94
Chanson H 1997 *Air Bubble Entrainment in Free-Surface Turbulent Shear Flows* (London: Academic) 401 p
Chanson H 2002 Air–water flow measurements with intrusive phase-detection probes. Can we improve their interpretation? *J. Hydraul. Eng.* **128** 252–5
Chanson H 2004 Unsteady air–water flow measurements in sudden open channel flows *Exp. Fluids* **37** 899–909
Chanson H 2005 Air–water and momentum exchanges in unsteady surging waters: an experimental study *Exp. Thermal Fluid Sci.* **30** 37–47
Chanson H 2007 Dynamic similarity and scale effects affecting air bubble entrainment in hydraulic jumps *Proc. 6th Int. Conf. on Multiphase Flow* (*Leipzig, Germany, 9–13 July 2007*) ed M Sommerfield, 11 p (CD-ROM)
Chanson H 2009 Turbulent air–water flows in hydraulic structures: dynamic similarity and scale effects *Environ. Fluid Mech.* **9** 125–42
Chanson H 2012 Momentum considerations in hydraulic jumps and bores *J. Irrigation Drainage Eng.* **138** 382–5
Chanson H 2013a Advective diffusion of air bubbles in turbulent water flows *Fluid Mechanics of Environmental Interfaces* 2nd edn, ed C Gualtieri and D T Mihailovic (Leiden: Taylor and Francis) chapter 7, pp 181–219
Chanson H 2013b Hydraulics of aerated flows: qui pro quo? *J. Hydraul. Res.* **51** 223–43
Chanson H, Aoki S and Hoque A 2002 Similitude of air bubble entrainment and dispersion in vertical circular plunging jet flows. An experimental study with freshwater, salty freshwater and seawater *Coastal/Ocean Engineering Report*, No. COE02-1, Department of Architecture and Civil Eng., Toyohashi University of Technology, Japan, 94 p
Chanson H, Aoki S and Hoque A 2006 Bubble entrainment and dispersion in plunging Jet flows: freshwater versus seawater *J. Coast. Res.* **22** 664–77
Chanson H and Brattberg T 1998 Air entrainment by 2D plunging jets: the impingement region and the very-near flow field *Proc. 1998 ASME Fluids Engineering Conf.* (*Washington DC, USA, 21–25 June 1998*) Keynote paper, Paper FEDSM98-4806, 8 p (CD-ROM)
Chanson H and Carosi G 2007 Advanced post-processing and correlation analyses in high-velocity air–water flows. *Environ. Fluid Mech.* **7** 495–508
Chanson H and Chachereau Y 2013 Scale effects affecting two-phase flow properties in hydraulic jump with small inflow Froude number *Exp. Thermal Fluid Sci.* **45** 234–42
Chanson H and Felder S 2010 Turbulence measurements in air–water self-aerated flows: basic analysis and results *Proc. 7th Int. Conf. on Multiphase Flow* (*Tampa FL, USA, 30 May–4June 4 2010*) Paper No. 10.3.4, 11 p (USB Memory Stick)
Chanson H and Gonzalez C A 2004 Interactions between free-surface, free-stream turbulence and cavity recirculation in open channel flows: measurements and turbulence manipulation *Proc. 5th Int. Conf. on Multiphase Flow* (*Yokohama, Japan*) ed Y Matsumoto *et al* Paper 104, 14 p
Chanson H and Toombes L 2002a Air–water flows down stepped chutes: turbulence and flow structure observations *Int. J. Multiph. Flow* **28** 1737–61
Chanson H and Toombes L 2002b Experimental study of gas–liquid interfacial properties in a stepped cascade flow *Environ. Fluid Mech.* **2** 241–63
Cox D T and Shin S 2003 Laboratory measurements of void fraction and turbulence in the bore region of surf zone waves *J. Eng. Mech.* **129** 1197–205
Crowe C, Sommerfield M and Tsuji Y 1998 *Multiphase Flows with Droplets and Particles* (Boca Raton, FL: CRC Press) 471 p
Clift R, Grace J R and Weber M E 1978 *Bubbles, Drops, and Particles* (San Diego: Academic) 380 p
Cummings P D 1996 Aeration due to breaking waves *PhD Thesis* Department of Civil Engineering, The University of Queensland, Brisbane, Australia
Ervine D A 1998 Air entrainment in hydraulic structures: a review *Proc. Institution of Civil Engineers, Water, Maritime and Energy* (*UK*) vol 130, pp 142–53
Ervine D A and Falvey H T 1987 Behaviour of turbulent water jets in the atmosphere and in plunge pools *Proc. Institution of Civil Engineers London* vol 83, pp 295–314 (Discussion: Part 2, Mar–June 1988, vol 85, pp 359–63)
Felder S 2013 Air–water flow properties on stepped spillways for embankment dams: Aeration, energy dissipation and turbulence on uniform, non-uniform and pooled stepped chutes *PhD Thesis* School of Civil Engineering, The University of Queensland, 506 p
Felder S and Chanson H 2009 Turbulence, dynamic similarity and scale effects in high-velocity free-surface flows above a stepped chute *Exp. Fluids* **47** 1–18
Felder S and Chanson H 2014 Triple decomposition technique in air–water flows: application to instationary flows on a stepped spillway *Int. J. Multiph. Flow* **58** 139–53
Felder S and Chanson H 2015 Phase-detection probe measurements in high-velocity free-surface flows including a discussion of key sampling parameters *Exp. Thermal Fluid Sci.* **61** 66–78
Gonzalez C 2005 Experimental study of free-surface aeration on embankment stepped chutes *PhD Thesis* The University of Queensland, Department of Civil Engineering, Brisbane, Australia, 240 p
Gualtieri C and Chanson H 2010 Effect of Froude number on bubble clustering in a hydraulic jump *J. Hydraul. Res.* **48** 504–8
Hager W H 1992 Energy dissipators and hydraulic jump *Water Science and Technology Library* vol **8** (Dordrecht: Kluwer Academic) 288 p
Heinlein J and Fritsching U 2006 Droplet clustering in sprays *Exp. Fluids* **40** 464–72
Henderson F M 1966 *Open Channel Flow* (New York: MacMillan)
Herringe R A 1973 A study of the structure of gas–liquid mixture flows *PhD Thesis* University of New South Wales, Kensington, Australia
Herringe R A and Davis M R 1974 Detection of instantaneous phase changes in gas–liquid mixtures *J. Phys. E: Sci. Instrum.* **7** 807–12
Hoque A and Aoki S 2005 Distributions of void fraction under breaking waves in the surf zone *Ocean Eng.* **32** 1829–40
Hoyt J W and Sellin R H J 1989 Hydraulic jump as 'mixing layer' *J. Hydraul. Eng.* **115** 1607–14
Hwung H H, Chyan J M and Chung Y C 1992 Energy dissipation and air bubbles mixing inside surf zone *Proc. 23rd Int. Conf. on Coastal Engineering* (*Venice, Italy*) vol 1, chapter 22, pp 308–21

Jones O C and Delhaye J M 1976 Transient and statistical measurement techniques for two-phase flows: a critical review *Int. J. Multiph.Flow* **3** 89–116
Kobus H 1984 Local air entrainment and detrainment *Proc. Int. Symp. on Scale Effects in Modelling Hydraulic Structures* (*Esslingen, Germany*)ed H Kobus, Paper 4.10, 10 p
Lance M and Bataille J 1991 Turbulence in the liquid phase of a uniform bubbly air–water flow *J. Fluid Mech.* **222** 95–118
Leandro J, Carvalho R, Chachereau Y and Chanson H 2012 Estimating void fraction in a hydraulic jump by measurements of pixel intensity *Exp. Fluids* **52** 1307–18
Leng X and Chanson H 2015 Turbulent advances of a breaking bore: preliminary physical experiments *Exp. Thermal Fluid Sci.* **62** 70–7
Liggett J A 1994 *Fluid Mechanics* (New York: McGraw-Hill)
Lighthill J 1978 *Waves in Fluids* (Cambridge: Cambridge University Press) 504 p
Liu T J and Bankoff S G 1993 Structure of air–water bubbly flow in a vertical pipe—II. Void fraction, bubble velocity and bubble size distribution *Int. J. Heat Mass Transfer* **36** 1061–72
Mossa M and Tolve U 1998 Flow visualization in bubbly two-phase hydraulic jump *J. Fluids Eng.* **120** 160–5
Murai Y, Oishi Y, Takeda Y and Yamamoto F 2006 Turbulent shear stress profiles in a bubbly channel flow assessed by particle tracking velocimetry *Exp. Fluids* **41** 343–52
Murzyn F and Chanson H 2008 Experimental assessment of scale effects affecting two-phase flow properties in hydraulic jumps *Exp. Fluids* **45** 513–21
Neal L S and Bankoff S G 1963 A high resolution resistivity probe for determination of local void properties in gas–liquid flows *Am. Inst. Chem. J.* **9** 49–54
Neal L S and Bankoff S G 1965 Local parameters in cocurrent mercury-nitrogen flow *Am. Inst. Chem. J.* **11** 624–35
Novak P and Cabelka J 1981 *Models in Hydraulic Engineering. Physical Principles and Design Applications* (London: Pitman)
Noymer P D 2000 The use of single-point measurements to characterise dynamic behaviours in spray *Exp. Fluids* **29** 228–37
Pfister M and Hager W H 2010 Chute aerators I: air transport characteristics *J. Hydraul. Eng.* **136** 352–9
Pothof I W M, Schuit A D and Clemens F H L R 2013 Influence of surface tension on air–water Flows *J. Hydraul. Eng.* **139** 44–50
Rajaratnam N 1965 The hydraulic jump as a wall jet *J. Hydraul. Div.* **91** 107–32 (Discussion: 92 110–23 & 93 74–6)
Rao N S L and Kobus H E 1971 Characteristics of self-aerated free-surface flows *Water and Waste Water/Current Research and Practice* vol 10 (Berlin: Eric Schmidt)
Reif T H 1978 The effects of drag reducing polymers on the turbulence characteristics of the hydraulic jump *Report* EW-11–78, US Naval Academy, Annapolis, USA, 50 p
Rensen J, Luther S and Lohse D 2005 The effect of bubbles on developed turbulence *J. Fluid Mech.* **538** 153–87
Rouse H, Siao T T and Nagaratnam S 1959 Turbulence characteristics of the hydraulic jump *Transactions* **124** 926–50
Salter M E, Nilsson E D, Butcher A and Bilde M 2014 On the seawater temperature dependence of the sea spray aerosol generated by a continuous plunging jet *J. Geophys. Res. Atmos.* **119** 21
Schultz M P and Flack K A 2013 Reynolds-number scaling of turbulent channel flow *Phys. Fluids* **25** 025104
Serizawa A, Kataoka I and Michiyoshi I 1975 Turbulence structure of air–water bubbly flows—I. Measuring techniques *Int. J. Multiph. Flow* **2** 221–33
Straub L G and Anderson A G 1958 Experiments on self-aerated flow in open channels *J. Hydraul. Div. Proc.* **84** 1890
Sun S and Chanson H 2013 Characteristics of clustered particles in skimming flows on a stepped spillway *Environ. Fluid Mech.* **13** 73–87
Toombes L 2002 Experimental study of air–water flow properties on low-gradient stepped cascades *PhD Thesis* University of Queensland, School of Civil Engineering, Brisbane, Australia, 304 p
Toombes L and Chanson H 2008 Interfacial aeration and bubble count rate distributions in a supercritical flow past a backward-facing step *Int. J. Multiph. Flow* **34** 427–36
Vejrazka J, Vecer M, Orvalho S, Sechet P, Ruzicka M C and Cartellier A 2010 Measurement accuracy of a mono-fiber optical probe in a bubbly flow *Int. J. Multiph. Flow* **36** 533–48
Wang H 2014 Turbulence and air entrainment in hydraulic jumps *PhD Thesis* School of Civil Engineering, The University of Queensland, Brisbane, Australia, 341 p & Digital appendices
Wang H, Felder S and Chanson H 2014 An experimental study of turbulent two-phase flow in hydraulic jumps and application of a triple decomposition technique *Exp. Fluids* **55** 1775
Wood I R 1983 Uniform region of self-aerated flow *J. Hydraul. Eng.* **109** 447–61
Wood I R 1991 Air entrainment in free-surface flows *IAHR Hydraulic Structures Design Manual No. 4, Hydraulic Design Considerations* (Rotterdam: Balkema) 149 p
Wuthrich D and Chanson H 2014 Aeration and energy dissipation over stepped gabion spillways: a physical study Hydraulic Model *Report No.* CH92/13 School of Civil Engineering, The University of Queensland, Brisbane, Australia, 171 p and 5 video movies